JMEPEG (2017) 26:3633–3647
DOI: 10.1007/s11665-017-2783-7

1059-9495/$19.00

Corrosion and Wear Behaviors of Cr-Doped Diamond-Like Carbon Coatings

S. Viswanathan, L. Mohan, Parthasarathi Bera, V. Praveen Kumar, Harish C. Barshilia, and C. Anandan

(Submitted December 28, 2016; in revised form April 21, 2017; published online June 20, 2017)

A combination of plasma-enhanced chemical vapor deposition and magnetron sputtering techniques has been employed to deposit chromium-doped diamond-like carbon (DLC) coatings on stainless steel, silicon and glass substrates. The concentrations of Cr in the coatings are varied by changing the parameters of the bipolar pulsed power supply and the argon/acetylene gas composition. The coatings have been studied for composition, morphology, surface nature, nanohardness, corrosion resistance and wear resistance properties. The changes in I_D/I_G ratio with Cr concentrations have been obtained from Raman spectroscopy studies. Ratio decreases with an increase in Cr concentration, and it has been found to increase at higher Cr concentration, indicating the disorder in the coating. Carbide is formed in Cr-doped DLC coatings as observed from XPS studies. There is a decrease in sp^3/sp^2 ratios with an increase in Cr concentration, and it increases again at higher Cr concentration. Nanohardness studies show no clear dependence of hardness on Cr concentration. DLC coatings with lower Cr contents have demonstrated better corrosion resistance with better passive behavior in 3.5% NaCl solution, and corrosion potential is observed to move toward nobler (more positive) values. A low coefficient of friction (0.15) at different loads is observed from reciprocating wear studies. Lower wear volume is found at all loads on the Cr-doped DLC coatings. Wear mechanism changes from abrasive wear on the substrate to adhesive wear on the coating.

Keywords corrosion, Cr-doped DLC, Raman spectroscopy, wear, XPS

1. Introduction

In periodic table, carbon has been regarded as one of the most important elements. It has the maximum number of allotropes, and more than 90% of chemicals contain carbon. Carbon-derived solid materials show unique properties such as super high hardness and thermal conductivity like in diamond or excellent lubricity and softness like in graphite. In last several years, carbon has also been used in the synthesis of diamond, diamond-like carbon (DLC) and carbon nitride coatings which have widely been used in engineering applications to control friction and wear because of their unique mechanical and tribological properties (Ref 1).

DLC coatings are metastable amorphous materials that have many properties similar to that of diamond. It contains *sp*, sp^2 and sp^3 hybridized carbon. These coatings are scientifically very fascinating and extremely important for numerous industrial applications due to their wide range of exceptional physical, chemical, mechanical and tribological properties (Ref 2-5). They are resistant to corrosive and oxidative attacks in acidic and saline media because of their excellent chemical inertness. While diamond is crystalline with complete carbon to carbon (C-C) sp^3 bonding, DLC is amorphous with varying degree of diamond-like properties that is highly dependent on the ratio of diamond sp^3 to graphitic sp^2 C-C bonds. However, the disadvantage of the DLC coating is poor adhesion to metal and metal alloys substrates due to its high internal stress which can be overcome by using interlayers and dopants (Ref 6).

In recent years, deposition of many metal-doped DLC coatings has been attempted to overcome poor adhesion and high residual stress of pure DLC coating (Ref 7-9). Nanocluster can be formed when metal atoms are incorporated into the DLC matrix or metal atoms are bonded with carbon atoms. It has been observed that metal-doped DLC coatings are formed with carbide-forming metals like Ti, W and Cr and non-carbide-forming metals like Cu, Ag and Pt. These transition metals modify the structure and help in improving mechanical and tribological properties of DLC coatings because of their d orbital that tends to overlap with *p* orbital of carbon (Ref 10-17). Among these dopant metals, Cr-doped DLC coating exhibits impressive tribological properties in comparison with undoped DLC coating because of their high adhesion and low stress. Research works on chromium interlayered and chromium-doped DLC coatings have been carried out by many groups, and they have investigated their thermal, mechanical, tribological, magnetic and electrical properties (Ref 18-36). However, detailed studies on electrochemical behavior on chromium-doped DLC coatings are limited in the literature. Wu et al. have studied corrosion characteristics of Cr-doped DLC coatings (Ref 37). But, detailed corrosion studies with electrochemical impedance spectroscopy (EIS) and equivalent circuit have not been attempted. In the present work, we report the development of Cr-doped DLC coatings using combined plasma-enhanced chemical vapor deposition (PECVD) and magnetron sputtering techniques. Furthermore, the effects of doping of chromium with DLC on the corrosion and wear behavior are also discussed.

S. Viswanathan, L. Mohan, Parthasarathi Bera, V. Praveen Kumar, Harish C. Barshilia and **C. Anandan,** Surface Engineering Division, CSIR-National Aerospace Laboratories, Bengaluru 560017, India. Contact e-mails: partho@nal.res.in and canandan@yahoo.com.

2. Experimental Details

2.1 Sample Preparation

Three different substrates were used in this study for studying different characterizations and properties. Silicon wafers (100) were cut into appropriate sizes and cleaned in acetone ultrasonically for x-ray photoelectron spectroscopy (XPS), nanohardness testing and Raman spectroscopy studies. Glass slides were cut into pieces and cleaned, and a portion was masked for thickness measurement by profilometer. Stainless steel (202) sheets were cut into 2 cm × 2 cm pieces and were grounded by silicon carbide emery papers of different grit sizes to smoothen their surfaces. After grinding substrates were polished to mirror-like finish with 0.3 μm alumina powder mixed in distilled water. The polished substrates were then ultrasonically cleaned for 15 min in acetone. These substrates were used for corrosion and wear studies.

2.2 Deposition of DLC and Cr-Doped DLC Coatings

The deposition chamber was pumped down to base vacuum of 5×10^{-6} mbar by a turbo-molecular pump backed with a rotary pump. The chamber and gas line were purged with process gases after reaching the base pressure. The source gases such as C_2H_2 and Ar were introduced into the chamber by a shower-head-type distributer, and flow rates were controlled by mass flow controllers (MKS Instruments, USA) and a throttle valve. The plasma was generated by 50 W RF power at 13.56 MHz frequency by inductive coupling. The samples were etched in hydrogen plasma for 10 min before deposition. Pure DLC was deposited with 100% of C_2H_2 plasma, and Cr-doped DLC was deposited with plasma of Ar and C_2H_2. Cr was sputtered from 99.95% pure Cr target using magnetron sputtering powered by a symmetric bipolar pulsed DC power supply from MAGPULS Stromversorgungs Systeme GmbH, Germany. Target parameters for sputter deposition of coatings with different Cr concentrations were 300-350 V bias voltage, 0.6 A bias current, 0.6 kW bias power and 50 kHz bias frequency. Pulse on and off times were 7 and 3 μs in both positive and negative channels. Substrates were biased with −110 V DC voltage for the deposition of all coatings. Gas composition and other parameters for the deposition of pure DLC and Cr-doped DLC coatings are summarized in Table 1.

2.3 Characterization

The coating thickness was measured by NanoMap500LS profilometer. Surface morphology of the coatings was obtained by FESEM with Carl Zeiss SUPRA 40 VP. Surface topography was investigated by AFM with CSEM Instruments (Model SSI) operated in contact mode. Raman spectra were collected using DILOR-JOBIN-YVON SPEX made LABRAM 010A with He-Ne laser source having wavelength of 632.8 nm. XPS of Cr-doped DLC coatings were recorded with a SPECS spectrometer, Germany, using non-monochromatic AlKα radiation (1486.6 eV) as an x-ray source operated at 150 W (12 kV, 12.5 mA). The binding energies reported here were referenced with C1s peak at 284.6 eV. All the individual spectra were recorded with a pass energy and step increment of 40 and 0.05 eV, respectively. For XPS recording, sample was mounted on a sample holder and placed into a load-lock chamber with an ultrahigh vacuum (UHV) of 8×10^{-8} mbar for 5 h in order to desorb any volatile species present on the surface. After 5 h, sample was transferred into the analyzing chamber with UHV of 5×10^{-10} mbar. Depth profiling studies were performed by sputtering the coatings with focused Ar^+ ion beam using IQE12/38 ion gun by applying energy of 2 keV with Ar gas pressure of 5×10^{-7} mbar for 5 and 10 min. The measured current during depth profiling studies by Ar^+ ion sputtering was 1 μA. C1s and Cr2p core level spectra were used to calculate the elemental concentrations of Cr-doped DLC coatings and were also curve-fitted with Gaussian-Lorentzian peaks to identify various carbon and chromium species after subtracting a Shirley background.

2.4 Properties

Nanohardness of substrate, pure DLC and Cr-DLC coatings was measured by using Nano Hardness Tester (CSM Instruments) with a Berkovich diamond indenter at 2 mN load.

Electrochemical studies of the substrate, pure DLC and Cr-doped DLC samples were carried out using CH 604D electrochemical workstation (CH Instruments, USA). A conventional three-electrode glass cell was used to conduct the electrochemical studies in 3.5% NaCl solution at room temperature. The sample, Pt foil and saturated calomel electrode (SCE) were used as the working electrode, counter electrode and reference electrode, respectively. The reference electrode was kept very close to the surface of the working electrode. The sample with 0.8 cm^2 area was immersed in 3.5% NaCl solution for 1 h to establish the open circuit potential (E_{OCP}). Electrochemical measurement has resulted in Tafel plot which is represented as log i versus potential plot. The corrosion potential (E_{corr}) and corrosion current density (i_{corr}) are obtained from the Tafel plot. The corrosion current is evaluated employing Stern-Geary equation (Ref 38).

$$i_{\text{corr}} = \frac{\beta_a \times \beta_c}{2.3R_{\text{p}}(\beta_a + \beta_c)} \quad \text{(Eq 1)}$$

where β_a and β_c are the Tafel slopes related to anodic and cathodic part of Tafel plot and R_p is polarization resistance. EIS measurement was taken in the frequency range from 10 mHz to 100 kHz. The applied alternating sinusoidal potential was 10 mV on the E_{OCP}. After each experiment, the impedance data were displayed as Bode plots. The Bode plot is a plot of log|Z| versus log f and −phase angle (θ) versus log f

Table 1 Pressure, gas composition, time, Cr concentrations and thicknesses of pure DLC and Cr-doped DLC coatings

Pressure, μbar	Argon:acetylene, sccm	Time, min	Cr concentration, at.%	Thickness, nm
11	10 (acetylene)	20	…	150
11	16:4	35	0.5	280
10	16:4	30	3.8	226
7.7	18:2	30	10.9	170
7.7	18:2	30	17.6	370

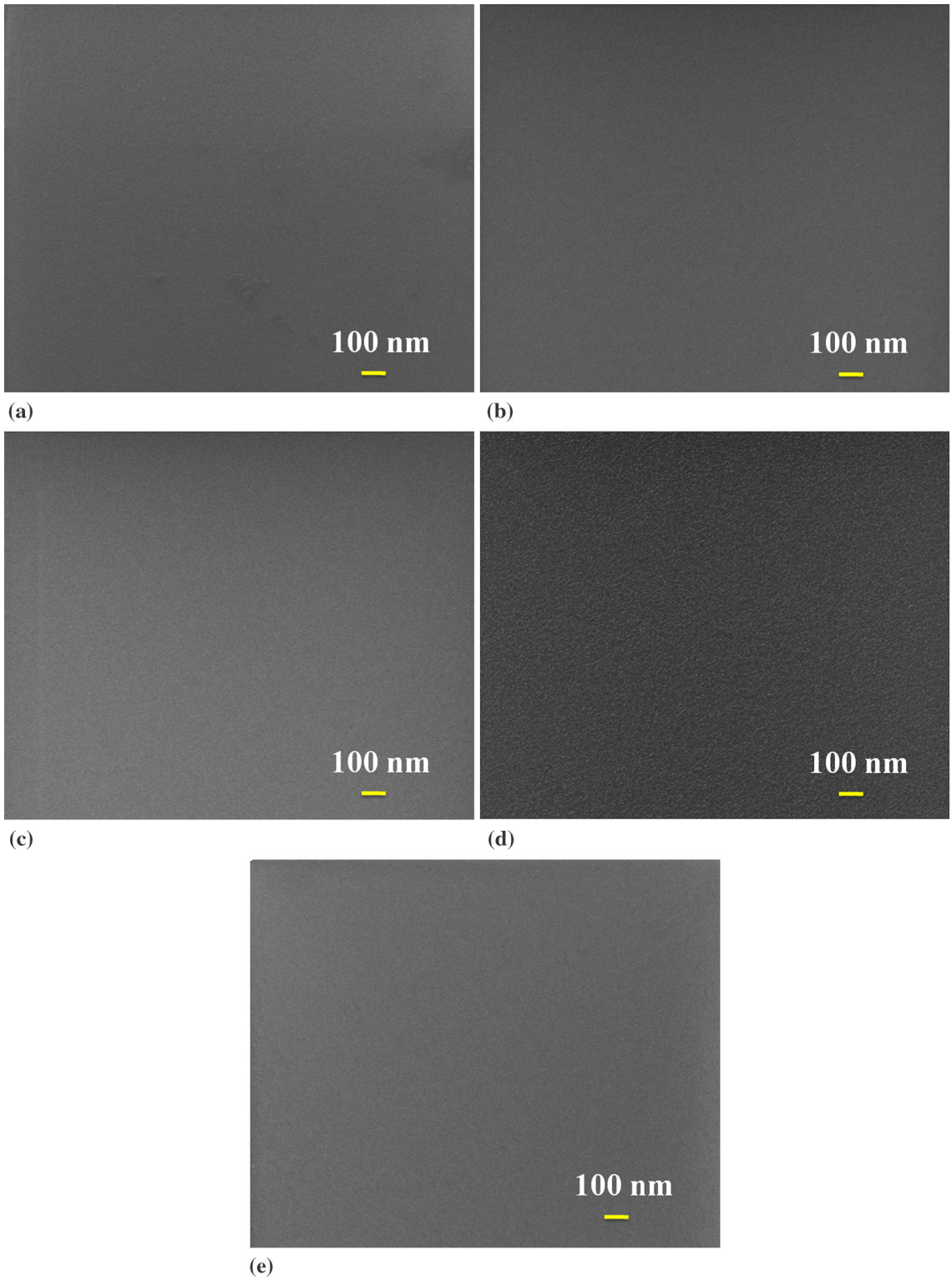

Fig. 1 FESEM images of Cr-doped DLC coatings with different Cr concentrations: (a) pure DLC (b) 0.5%, (c) 3.8%, (d) 10.9% and (e) 17.6%

where $|Z|$ and f are absolute impedance and frequency, respectively. The acquired data were curve-fitted and analyzed using ZSimpwin program (Princeton Applied Research, USA) to obtain suitable equivalent circuit parameters. The fitting quality was checked by the χ^2 value. After EIS measurements, potentiodynamic polarization studies were carried out in a potential range of 200 mV below and above the OCP value with a scan rate of 1 mV s^{-1}.

Wear studies of bare substrate and 3.8% Cr-doped DLC-coated substrate were carried out in a reciprocating wear tester

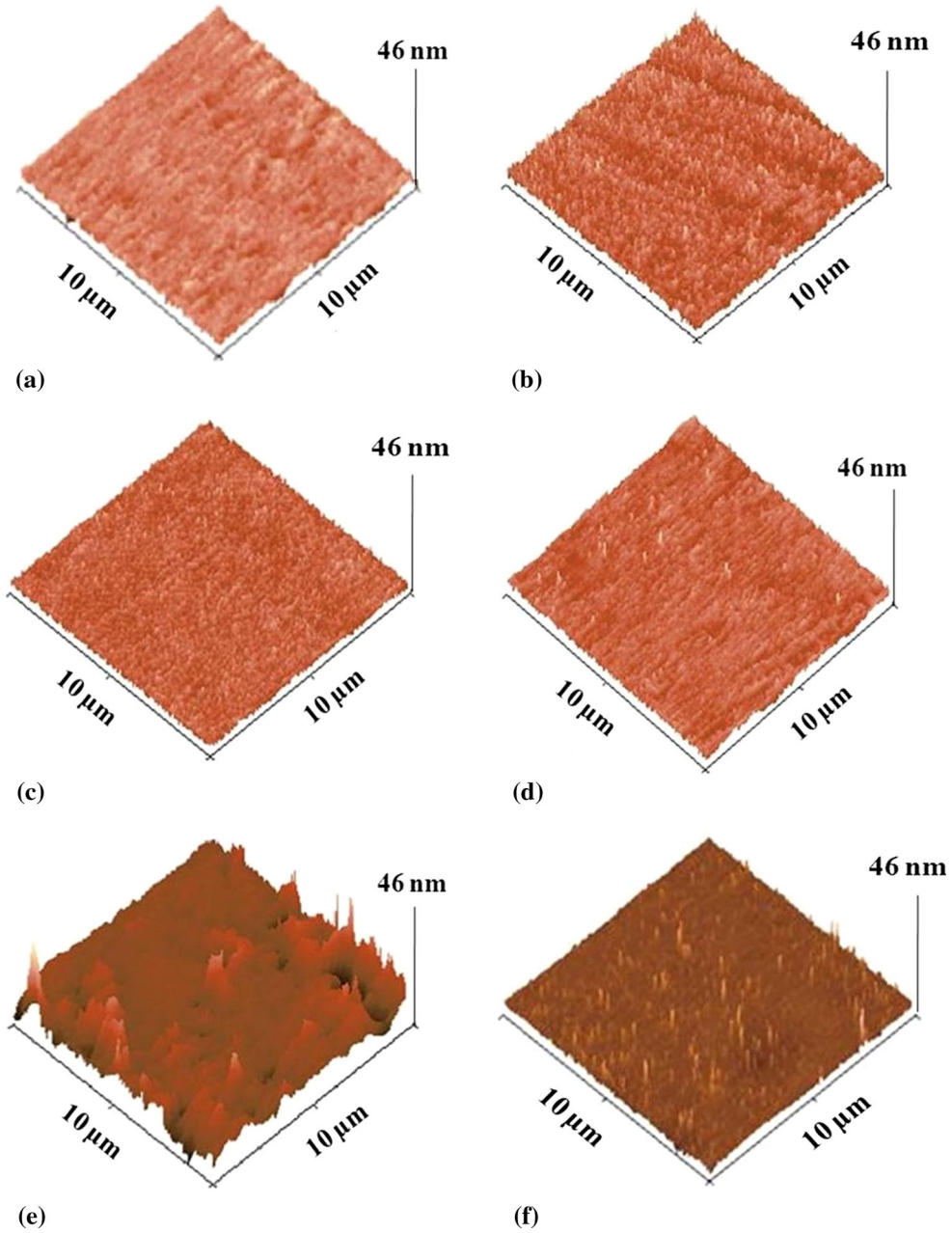

Fig. 2 AFM images of (a) substrate, (b) pure DLC, (c) 0.5% Cr-DLC, (d) 3.8% Cr-DLC, (e) 10.9% Cr-DLC and (f) 17.6% Cr-DLC coatings

(Model CM 9084 DuCom) as per ASTM G133-02 standards (Ref 39). However, these tests are not in full compliance with the provisions of Test Method G 133, Procedure A, because the normal forces in these experiments were 2, 5 and 7 N instead of 25 N as prescribed by the standard. Also, the stroke length was 10 mm and an alumina ball of 6 mm diameter was used as the counter surface. Further, the experiments were carried out at a frequency of 100 Hz and each experiment duration was 20 min. Relative humidity during tribology measurements was around 65%. After the experiments, wear profiles of the samples were examined by a profilometer. Considering ASTM G133-02 method the wear losses were calculated from the cross-sectional areas of the respective wear profiles (Ref 40).

3. Results and Discussion

3.1 Composition and Thickness

In our previous study, it has been found that pure DLC deposited on Ti alloy substrate by PECVD does not adhere to the substrate without an interlayer (Ref 40). Undoped DLC starts to peel off from the substrate after some time. However, we have also reported that Zr- and Mo-doped DLC coatings with graded Zr/Mo composition improves the adhesion to the titanium substrates (Ref 40-42). Table 1 shows the Cr concentrations (at.%) obtained from XPS studies. The concentrations of Cr in the coatings vary from

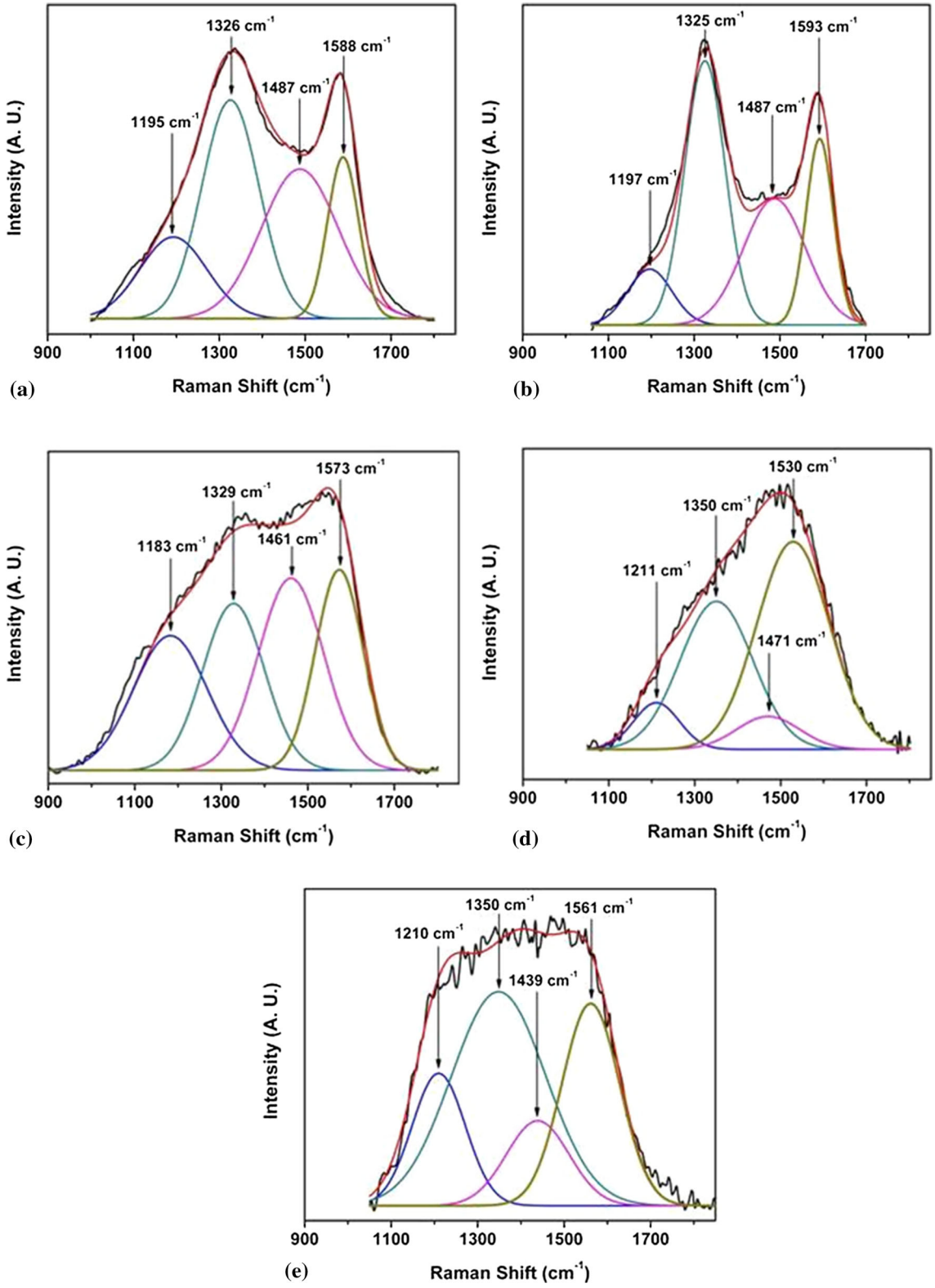

Fig. 3 Raman spectra of (a) pure DLC, (b) 0.5% Cr-DLC, (c) 3.8% Cr-DLC, (d) 10.9% Cr-DLC and (e) 17.6% Cr-DLC coatings

0.5 to 17.6 at.% depending on the process gas composition and the pulse on/off times of the bipolar pulsed power supply. The thicknesses of the films are obtained from profilometry by masking a portion of the glass substrate. The thicknesses of pure and Cr-doped DLC coatings range from 150 to 370 nm. To obtain different Cr concentrations different deposition parameters have been considered while depositing the coatings.

Table 2 I_D/I_G ratios, sp^3/sp^2 ratios, nanohardness, Young's modulus and indentation depth of substrate, pure DLC and Cr-doped DLC samples

Samples	I_D/I_G	sp^3/sp^2	Hardness, GPa	Young's modulus, GPa	Indentation depth, nm
Substrate	…	…	13.1 ± 1.2	145 ± 10.3	135
Pure DLC	1.11	1.37	21.1 ± 1.5	161 ± 13.3	86
0.5% Cr-DLC	1.02	1.29	18.3 ± 0.5	141 ± 2.6	97
3.8% Cr-DLC	0.91	0.79	22.6 ± 0.5	190 ± 1.1	89
10.9% Cr-DLC	0.75	0.41	14.8 ± 0.7	154 ± 1.5	96
17.6% Cr-DLC	1.61	2.85	20.4 ± 0.6	172 ± 2.5	91

3.2 FESEM Studies

FESEM images of the pure DLC and Cr-doped DLC coatings with higher magnifications are shown in Fig. 1(a), (b), (c), (d) and (e) for different Cr concentrations. The coatings show a compact and dense microstructure. Coatings with lower Cr concentrations show smooth amorphous surface morphologies similar to pure DLC coating as observed in Fig. 1(a), (b) and (c), whereas coatings with higher Cr concentrations contain some nanoroughness as shown in Fig. 1(d) and (e). These results are consistent with our previous studies for zirconium-doped DLC (Ref 40). However, no localized delamination of the coatings is observed in all samples.

3.3 AFM Studies

Figure 2 shows surface topographies of the silicon substrate, pure DLC coating and DLC coatings with different Cr concentrations. AFM images reveal that all the coatings possess smooth surface. However, nanoscale roughness on coated samples has been observed. The average roughness (R_a) values of silicon substrate, pure DLC, 0.5% Cr-DLC, 3.8% Cr-DLC, 10.9% Cr-DLC and 17.6% Cr-DLC coatings are 0.44, 0.69, 0.51, 0.36, 1.38 and 0.81 nm, respectively. It is observed that 10.9% Cr-doped DLC coating shows higher roughness value of 1.38 nm compared to all other coatings that is similar to features in FESEM images.

3.4 Raman Spectroscopy Studies

The Raman spectra of different Cr-doped DLC and pure DLC coatings on silicon are shown in Fig. 3. For estimating I_D/I_G ratios of the coatings Raman spectra have been curve-fitted with Gaussian-Lorentzian peaks. Normally, two peaks are used to fit Raman spectra of DLC coatings in the range from 1100 to 1700 cm^{-1}. However, it has been suggested that four Gaussian peaks are required for good fitting of the Raman spectra of DLC (Ref 33, 43, 44). Raman spectra of Cr-doped DLC are fitted with four peaks ($D1$, $D2$ and $G1$, $G2$). These four peaks are consigned around ~1350 cm^{-1} for $D1$ peak, which corresponds to microcrystalline or nanocrystalline graphite, and peak around ~1180 cm^{-1} for $D2$ peak, which is nanocrystalline diamond. The peak around ~1490 cm^{-1} for $G1$ peak, is related to disordered graphite, and ~1580 cm^{-1} for $G2$ peak, corresponds to ordered graphite (Ref 43). These peaks are characteristic of DLC structure (Ref 33, 43-46). The ratio of the amplitudes of the $D1$ and $D2$ peaks and the $G1$ and $G2$ peaks is used to estimate the I_D/I_G ratio. The ratio has been calculated on these peak intensities using $D = D1 + D2$ and $G = G1 + G2$ (Ref 43). The I_D/I_G values represent the degree of disorder in the carbon network. The I_D/I_G ratios lie in between 1.35 and 0.6 for pure DLC and different Cr-doped DLC coatings and are listed in Table 2. The I_D/I_G ratios of pure DLC and 0.5% Cr-DLC coatings are more or less similar, and it decreases with an increase in Cr concentrations up to 10.9% Cr. However, the ratio increases with an increase in Cr concentration to 17.6% and therefore suggests that the disorder in the material increases with increasing metal concentration in the DLC coating (Ref 46).

3.5 XPS Studies

Detailed XPS characterization has been carried out to understand the surface nature of pure DLC and Cr-doped DLC coatings. C1s core level spectral envelopes of pure DLC and different Cr-DLC coatings are broad and asymmetrical, indicating the presence of several carbon components in the coatings which are curve-fitted into several component peaks. Figure 4 displays curve-fitted C1s core level spectra of pure DLC and different Cr-DLC coatings. Accordingly, peaks at 283.1, 284.5, 285.3, 287.7 and 289.4 eV observed in the coatings are attributed to carbide, sp^2 carbon (C=C), sp^3 carbon (C-C), C=O and CO_3^{2-} species, respectively (Ref 47-50). Ratios of sp^3/sp^2 in all coatings have been calculated from the areas under the respective peaks that is summarized in Table 2. It is observed that sp^3/sp^2 ratio decreases with an increase in Cr concentrations. At very high Cr concentration it increases again. This observation agrees well with the Raman spectroscopy studies.

Figure 5 shows Cr2p core level spectra of Cr-doped DLC coatings. It can be seen from the figure that spectral natures of Cr2p are broad, indicating that Cr is present in various oxidation states in Cr-doped DLC coatings. Cr2p core level spectra of Cr-DLC coatings are resolved into two sets of spin-orbit doublets. Curve-fitted Cr2p core level spectra of 3.8 and 17.9% Cr-doped DLC coatings are also presented in Fig. 5. Accordingly, $Cr2p_{3/2,1/2}$ peaks observed at 574.4 and 583.8 eV in the curve-fitted spectra are ascribed to Cr carbide species, whereas peaks at 576.7 and 585.9 eV as observed correspond to oxidized Cr^{3+} species. All these values of Cr carbide and Cr^{3+} species are close to the values reported in the literature (Ref 51-53). Comparing the intensities of Cr carbide and Cr^{3+} related peaks in the curve-fitted spectrum it has to be noted that around 44% of total Cr is in Cr carbide form and the rest of Cr is present as Cr^{3+} species in 3.8% Cr-DLC coating. On the other hand, 75% Cr carbide and 25% oxidized Cr are observed in 17.6% Cr-DLC coating. It is noticed that Cr is present mainly in oxidized state in the coatings contained with lower amount of Cr, whereas it is in carbide form in higher Cr content coatings. Relative surface concentrations of Cr with respect to carbon have been evaluated from XPS studies and are given in Table 1. It is important to mention that the initial decrease in sp^3/sp^2 ratio is due to the Cr doping which can be attributed to the

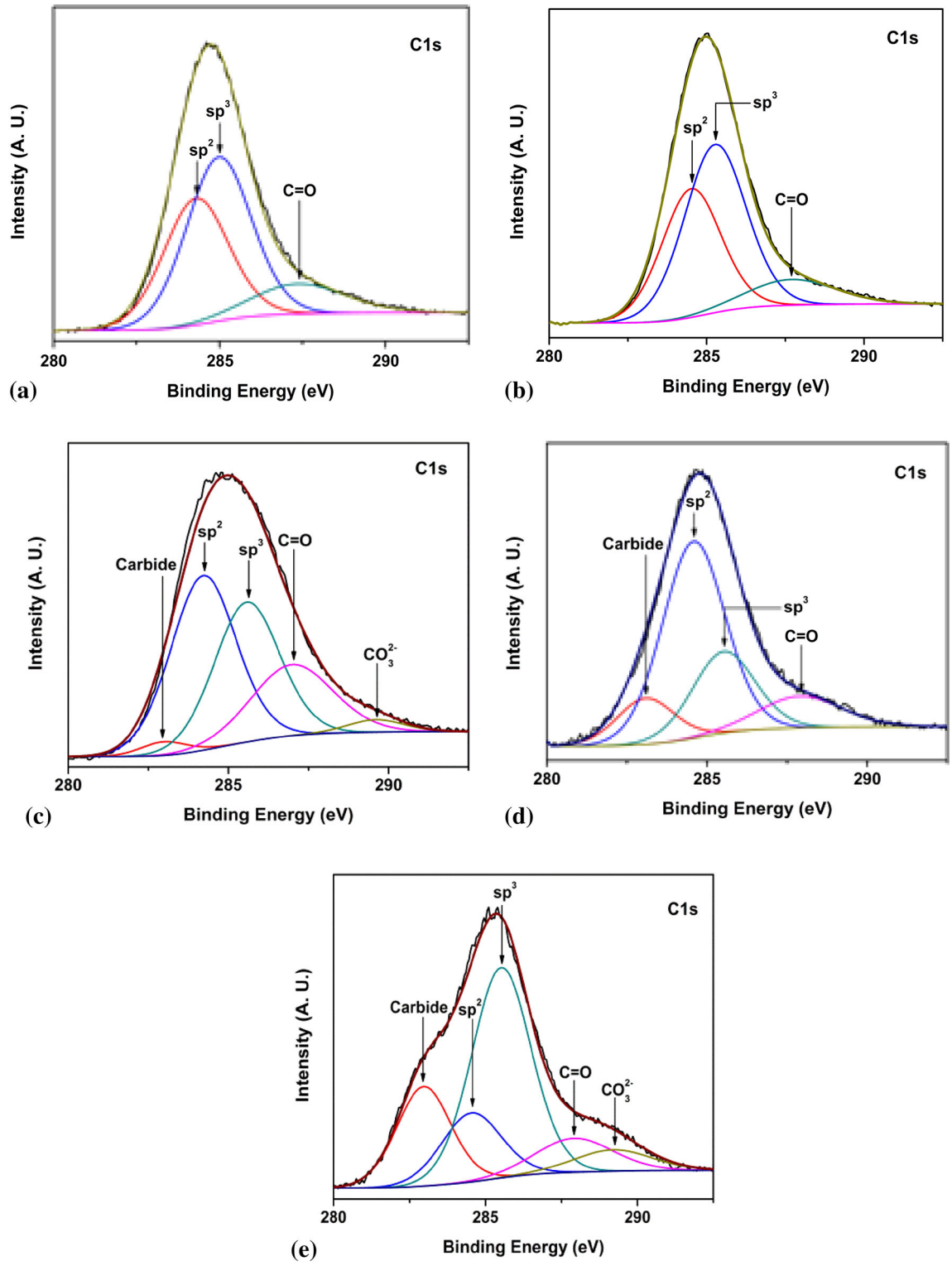

Fig. 4 C1s core level spectra of (a) pure DLC, (b) 0.5% Cr-DLC, (c) 3.8% Cr-DLC, (d) 10.9% Cr-DLC and (e) 17.6% Cr-DLC coatings

catalyst effect of Cr atoms on the formation of sp^2 sites. As sp^2 carbon has lower binding energy compared to sp^3 carbon, it prefers to bond with Cr to form Cr carbide phase. Because of this, a significant numbers of sp^2 carbon are used to form Cr carbide phase resulting in the decrease in sp^2 fraction of carbon which in turn increases sp^3/sp^2 ratio in DLC coatings with higher amount of Cr (Ref 19). Similar type of increase in sp^3/sp^2 ratio is reported for Mo-DLC coating (Ref 54). Thus, results obtained from XPS studies are also corroborated with Raman spectroscopy studies discussed in previous section.

To understand the composition of in the subsurface regions, depth profiling studies of the coatings using XPS have also been carried out. Cr2p core level spectra of 3.8 and 17.6% Cr-DLC coatings after depth profiling experiments are shown in

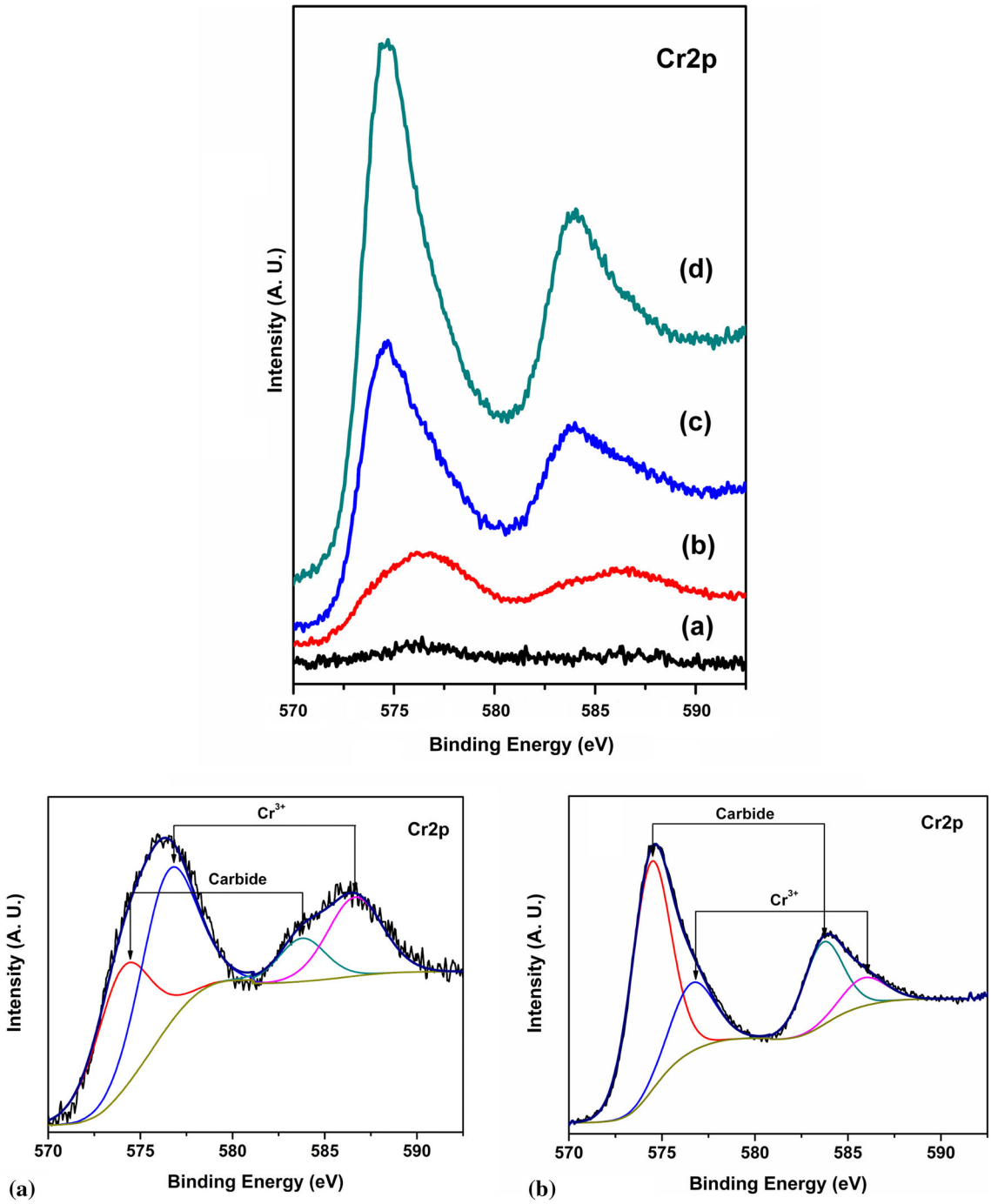

Fig. 5 Top: Cr2p core level spectra of (a) 0.5% Cr-DLC, (b) 3.8% Cr-DLC, (c) 10.9% Cr-DLC and (d) 17.6% Cr-DLC coatings. Bottom: curve-fitted Cr2p core level spectra of (a) 3.8% Cr-DLC and (b) 17.6% Cr-DLC coatings

Fig. 6. It has been observed that Cr is mainly present in carbide form after successive sputtering in both the coatings. It is also important to note that concentrations of Cr increase after first sputtering and are observed to be same after second successive sputtering in both the coatings.

3.6 Nanohardness Studies

Nanohardness measurements have been taken on uncoated silicon substrate, pure DLC and Cr-doped DLC-coated silicon samples at 2 mN loads. Figure 7 shows variation of hardness and Young's modulus with Cr concentrations. The average hardnesses along with Young's modulus of the coatings are summarized in Table 2. It can be found that uncoated silicon substrate has hardness of 13 ± 1.2 GPa with indentation depth of 135 nm. The hardness values of pure DLC and Cr-DLC coatings are varied from 15 to 22 GPa. In the case of pure DLC coating, hardness and depth of indentation are 21.1 ± 1.5 GPa and 86 nm, respectively. Indentation depth of Cr-doped DLC-coated samples is in the range from 86 to 97 nm that is given in Table 2. According to the table, no clear dependence of hardness on Cr concentrations is observed. This is possibly

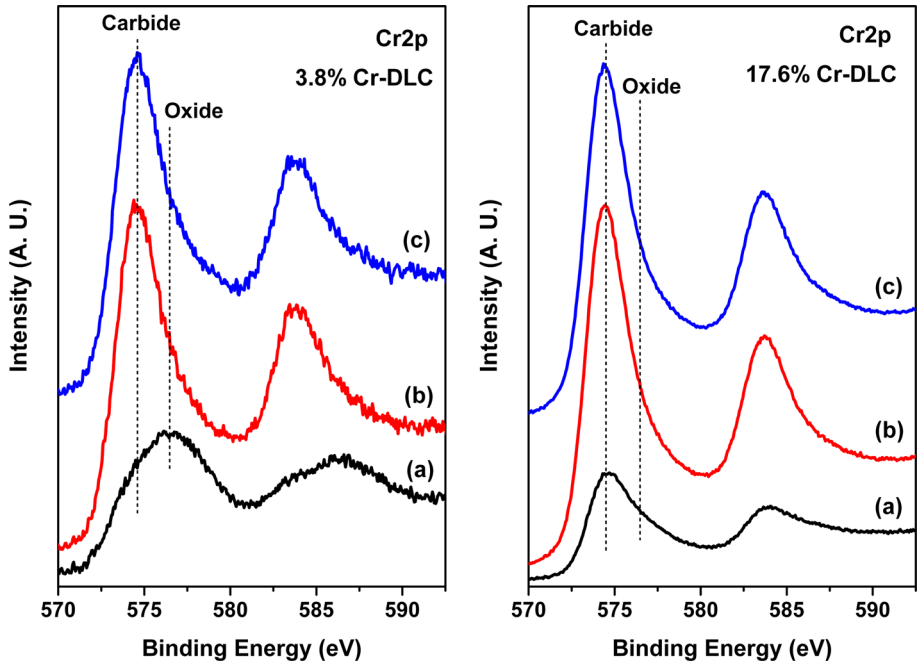

Fig. 6 Cr2p core level spectra of 3.8% Cr-DLC and 17.6% Cr-DLC coatings with different stages of sputtering: (a) as-deposited, (b) after 5 min sputtering and (c) after 10 min sputtering

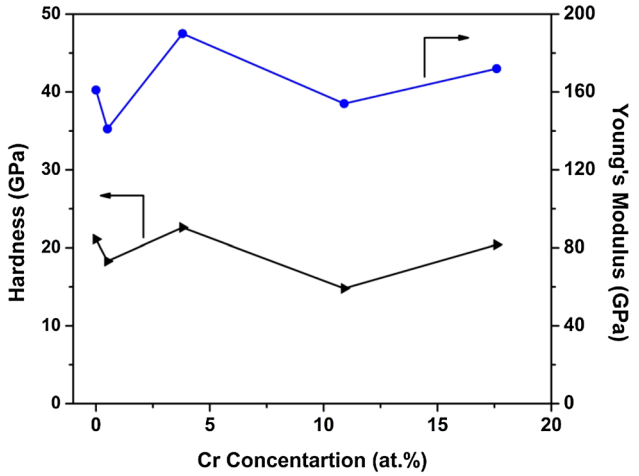

Fig. 7 Variation of hardness and Young's modulus in Cr-doped DLC coatings

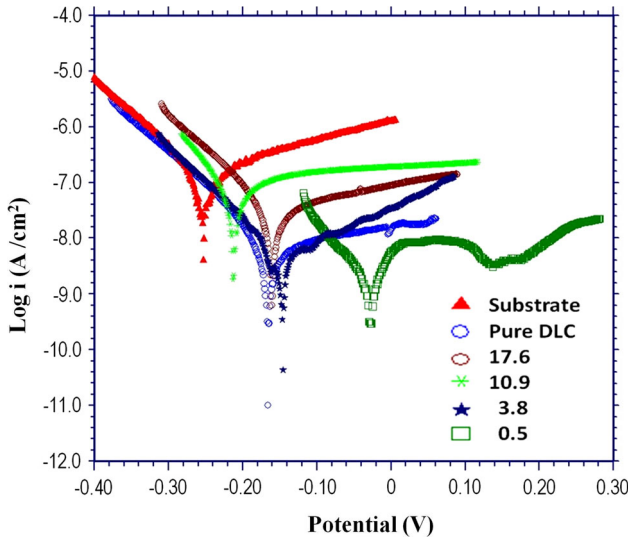

Fig. 8 Potentiodynamic polarization curves of substrate, pure and Cr-doped DLC-coated substrates

linked with the change in intrinsic strain during inclusion of metal phase in DLC coating which is observed in Ag impregnation in DLC coating (Ref 55). Previous works have also reported the softening of DLC coatings with metal doping (Ref 56-59). In the present study, 3.8% Cr-doped DLC shows better hardness (22.6 ± 0.5 GPa) with indentation depth of 89 nm compared to that of other doping concentrations and its Young's modulus is 190 ± 1.1 GPa. Hardness and Young's modulus values of 13.5 and 165 GPa are observed in Cr-DLC coating obtained with linear ion beam technique in the work of Dai et al. (Ref 18). They have also reported hardness and Young's modulus values of 12 and 155 GPa in Cr-DLC coating obtained by hybrid beam technique (Ref 21). Wu et al. have reported hardness value of 26 GPa in Cr-DLC coating deposited with high-power pulsed magnetron sputtering (Ref 37).

Table 3 Results of potentiodynamic polarization studies of substrate, pure DLC and Cr-doped DLC samples

Samples	E_{corr}, V	i_{corr}, μA cm^{-2}
Substrate	−0.236	0.0919
Pure DLC	−0.165	0.0038
0.5% Cr-DLC	−0.027	0.0052
3.8% Cr-DLC	−0.148	0.0059
10.9% Cr-DLC	−0.213	0.0841
17.6% Cr-DLC	−0.161	0.0238

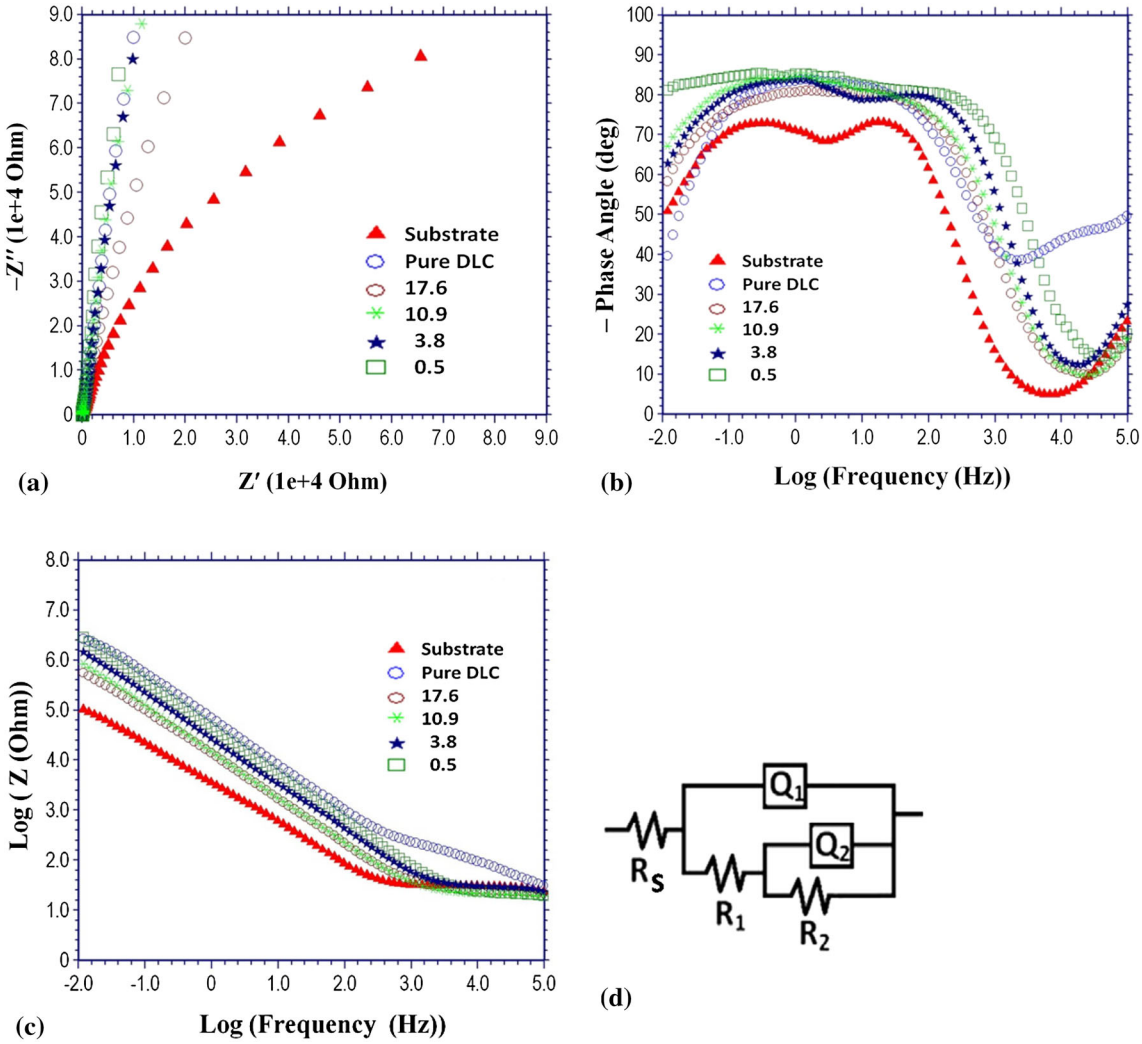

Fig. 9 (a) Nyquist plots, (b) Bode phase angle plots, (c) Bode plots and (d) equivalent circuit diagram used for fitting EIS data for substrate, pure and Cr-doped DLC coatings

Table 4 Electrochemical impedance parameters obtained by fitting equivalent circuit model for substrate and Cr-doped DLC samples

Samples	R_s, Ω cm^2	Q_1, S s^n cm^{-2}	n_1	R_1, Ω cm^2	Q_2, S s^n cm^{-2}	n_2	R_2, Ω cm^2	χ^2
Substrate	9.5	3.6×10^{-5}	0.87	25	5.2×10^{-8}	0.93	1.6×10^{6}	1.9×10^{-3}
Pure DLC	15	8.2×10^{-7}	0.82	212	1.8×10^{-6}	0.94	4.2×10^{6}	5.1×10^{-3}
0.5% Cr-DLC	15	1.9×10^{-6}	0.86	20	1.2×10^{-5}	0.91	3.2×10^{6}	1.0×10^{-3}
3.8% Cr-DLC	7	6.7×10^{-6}	0.92	23	5.6×10^{-8}	0.93	4.3×10^{6}	1.4×10^{-3}
10.9% Cr-DLC	12	2.3×10^{-6}	0.92	22	3.9×10^{-6}	0.92	1.8×10^{6}	2.5×10^{-3}
17.6% Cr-DLC	10	2.3×10^{-6}	0.65	27	1.2×10^{-5}	0.91	1.8×10^{6}	1.9×10^{-3}

3.7 Electrochemical Studies

In Fig. 8, potentiodynamic polarization curves of the substrate, pure DLC and different Cr-doped DLC-coated substrates in 3.5% NaCl solution are presented. The corrosion current density (i_{corr}) has been obtained by extrapolation of the anodic and cathodic branches of the polarization curves to the corrosion potential using Eq 1. Table 3 summarizes the corrosion current density and corrosion potential for the substrate, pure DLC and Cr-doped DLC-coated substrates. The observed corrosion current density (i_{corr}) for substrate is 0.0919 μA cm^{-2} which is higher than the pure DLC and different Cr-doped DLC-coated substrates. This indicates that coatings increase the corrosion resistance of the substrate. It is also shown in Fig. 8 that the current for formation of a passive layer is lower for the pure DLC and Cr-doped DLC-coated samples as compared to that of substrate. This shows that the pure DLC and Cr-doped DLC coatings have better passivation compared to that of the substrate. The E_{corr} values are shifted to much nobler value for

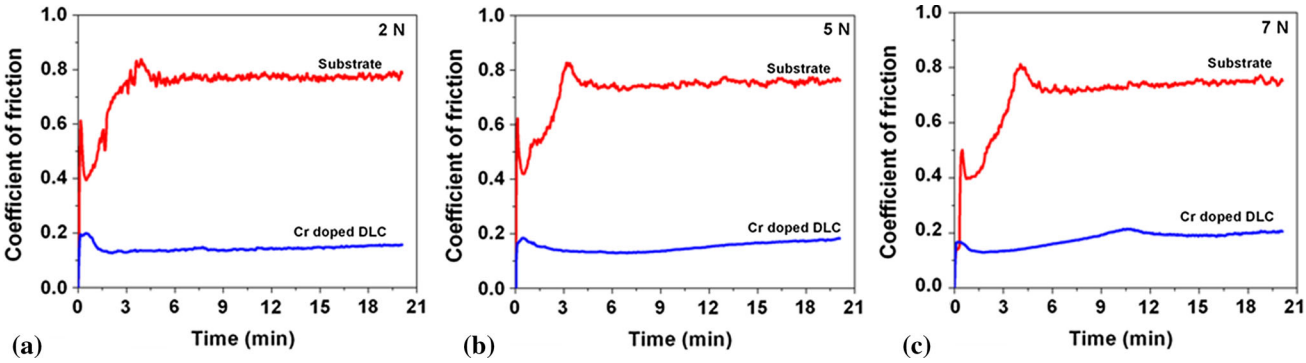

Fig. 10 Plots of coefficient of friction vs. time on substrate and 3.8% Cr-doped DLC-coated substrate at (a) 2 N, (b) 5 N and (c) 7 N loads

pure DLC and different Cr-doped DLC samples in comparison with the substrate value of −0.236 V. The values of E_{corr} given in Table 3 show that Cr-doped DLC coatings possess good resistance for corrosion. An increase in the concentration of Cr doping results in slight change in corrosion resistance. Pure DLC and 0.5% Cr-DLC coatings show higher corrosion resistance compared to that of 3.8, 10.9 and 17.6% Cr-DLC coatings. This can be due to the fact that DLC has higher corrosion resistance.

In Fig. 9, electrochemical impedance spectroscopy results in 3.5% NaCl solution are displayed in the form of Nyquist and Bode plots. The Nyquist plots in Fig. 9(a) are semicircular with the substrate, pure DLC and Cr-doped DLC coatings wherein Cr-doped DLC coatings have larger diameters in higher and lower frequencies. The limiting impedance at the high-frequency end corresponds to solution resistance (R_s). In Bode phase angle plot in Fig. 9(b), for substrate, the phase angle changes rapidly from −0° to −20° in the high-frequency range (10 to 100 kHz). In the low-frequency range from 0.01 to 100 Hz, the phase angle remains nearly constant around −78° that is lower than −90°, the value for an ideal capacitor. In the same frequency range, a linear relationship between log $|Z|$ and log f is noticed with a slope close to one (Fig. 9c). In the case of pure DLC, there is a rapid change in the phase angle from −50° to −40° in the high-frequency range (10 to 100 kHz); however, at low-frequency range (0.01 Hz to 100 Hz), the phase angle remains nearly constant around −80° that is lower than −90°, the value for an ideal capacitor. In the case of Cr-doped DLC coatings, as shown in Fig. 9(b), the phase angle in the frequency range from 0.1 Hz to 100 Hz is −84° and slightly decreases in the lower-frequency range.

The equivalent circuit (EC) model employed for fitting the EIS data of the substrate, pure DLC and Cr-doped DLC-coated samples is presented in Fig. 9(d). The equivalent electrochemical circuit consists of resistances and constant phase elements (CPE). In the fitting procedure, the non-ideal capacitive response of the oxide layers is entailed employing a constant phase element instead of a pure capacitance. This CPE is because of the difference in the relaxation times as a result of different degrees of surface inhomogeneity. The impedance with the capacitance is defined as $Z_{CPE} = [Q\,(j\omega^n)]^{-1}$, where Q, j, ω and n are the pseudo-capacitance or non-ideal capacitance, imaginary function ($\sqrt{-1}$), angular frequency and the deviation from the ideal behavior of a pure capacitor, respectively. When $n = 1$, the system behaves like a pure capacitor and $Q = C$ where C represents capacitance. In the EC, the resistive components R_s, R_1 and R_2 are related to the solution resistance, outer porous layer resistance and inner layer resistance, respectively. Q_1 is the capacitance of the outer layer, and Q_2 is the capacitance of the inner layer (Ref 40). In the case of coated sample, the equivalent circuit is same as that of the substrate with the outer porous oxide layer replaced by roughness and/or DLC coating with pinholes which play the role of pores in the oxide. The values of the electrical parameters obtained by fitting the impedance data of the substrate, pure DLC and Cr-doped DLC samples are given in Table 4. For the substrate, the resistance of outer porous layer (R_1) is observed to be 25 Ω cm^2. High corrosion resistance (R_2) of 1.6×10^6 Ω cm^2 observed on the substrate is associated with inner oxide layer. The Q_2 component is related to the capacitance of this inner barrier layer. The value of n for the constant phase element representing the outer layer is 0.87 and that representing the inner layer is 0.93. Table 4 shows high R_2 values for pure DLC and Cr-doped DLC coatings, indicating that they possess good corrosion resistance. The barrier layer (DLC/Cr-doped DLC layer) resistance of coated samples is higher compared to that of substrate one. This can be due to DLC and doping of DLC with metal. In addition to the above, it is well known that doping of DLC with metals improves its adhesion to substrate and also improves their tribological properties.

3.8 Wear Studies

Among different Cr-doped DLC coatings, 3.8% Cr-doped DLC has resulted in good hardness and better corrosion resistance. Hence, reciprocating wear studies have been carried out for 3.8% Cr-doped DLC coating and compared with the bare substrate at different loads. The evaluation of coefficient of friction (COF) on the bare stainless steel substrate and 3.8% Cr-doped DLC coating for different loads in a linear reciprocating wear test is shown in Fig. 10. COF graph of the substrate has two regions. In first region, the COF has low values of 0.4-0.6 and increases gradually, especially after 5 min at 2, 5 and 7 N loads. The COF for the 3.8% Cr-doped DLC is 0.15-0.16 initially and does not change significantly with load. Dai et al. have reported COF value of 0.3 in Cr-DLC coating deposited by hybrid beam technique which is lower than magnesium alloy substrate value of 0.4 (Ref 19). They have also observed COF value of 0.15 in DLC coating on silicon wafer with low Cr concentration deposited by hybrid beam technique (Ref 21). Wu et al. have reported COF values of 0.09-0.22 in Cr-DLC coatings deposited by high-power pulsed magnetron sputtering (Ref 37).

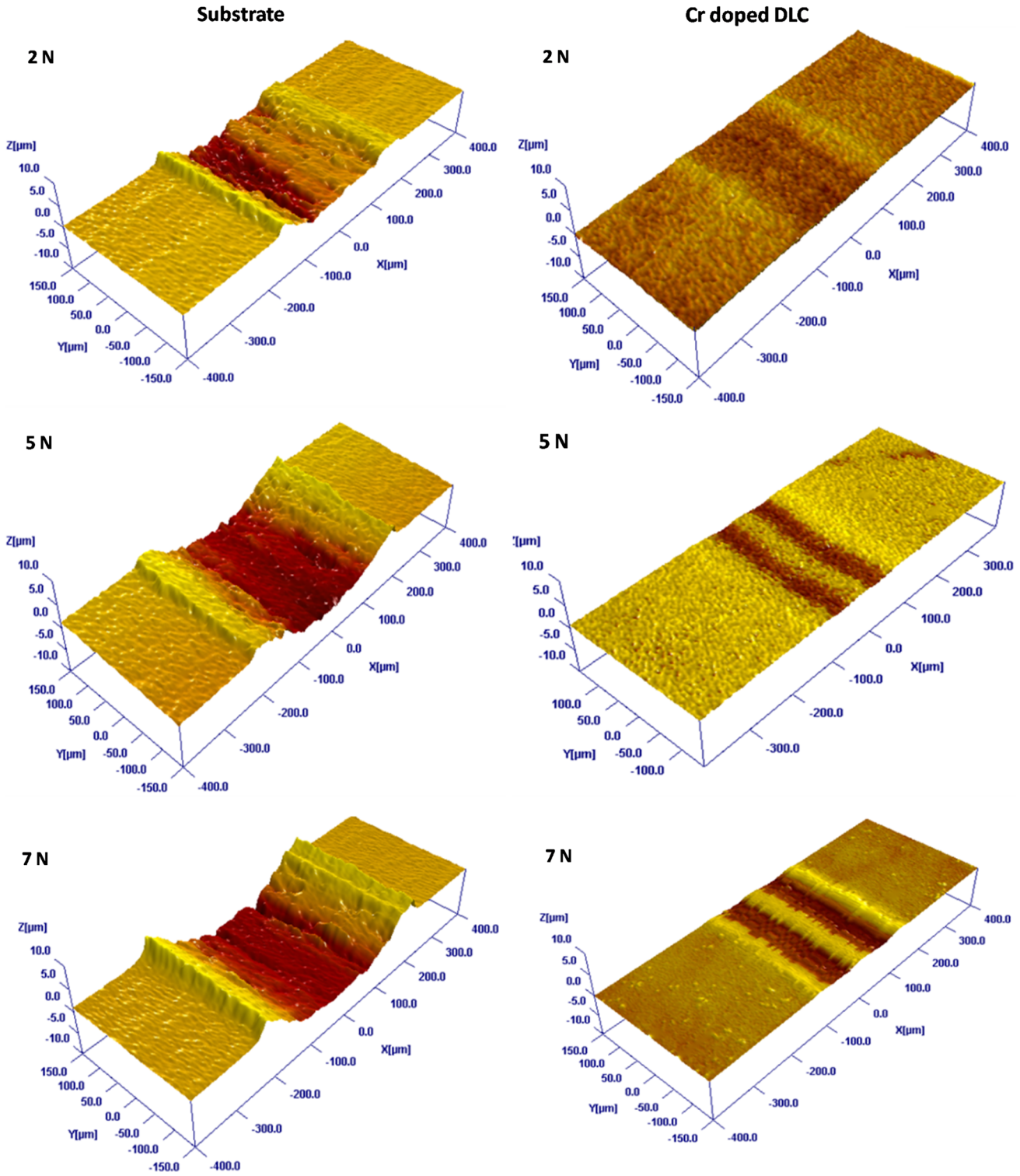

Fig. 11 3D profiles of wear tracks at 2, 5 and 7 N loads on substrate and 3.8% Cr-doped DLC-coated substrate

Figure 11 and 12 represent the 3D and 2D profiles of wear tracks for 2, 5 and 7 N loads on substrate and 3.8% Cr-doped DLC coatings, respectively. It can be noticed from the figures that the wear tracks on the substrate have deep grooves, whereas the wear tracks on the 3.8% Cr-doped DLC appear less deep. The average wear loss given in Table 5 shows that 3.8% Cr-doped DLC reduces the wear loss. In the case of substrate, the wear loss is 0.010 to 0.016 mm^3 at 2 to 5 N loads, respectively. Wear loss doubles to 0.022 mm^3 when increasing the load from 2 N to 7 N. In case of 3.8% Cr-doped DLC, the wear loss is negligible (0.00014 mm^3) at 2 N load and slightly increases to 0.0008 and 0.0012 mm^3 at 5 and 7 N, respectively, and the effect of increasing load on wear loss is also not significant. It has been observed that the wear loss of the coated substrate is less than that of the substrate and wear marks are also found to be shallower. These observations indicate a change in the wear mechanism

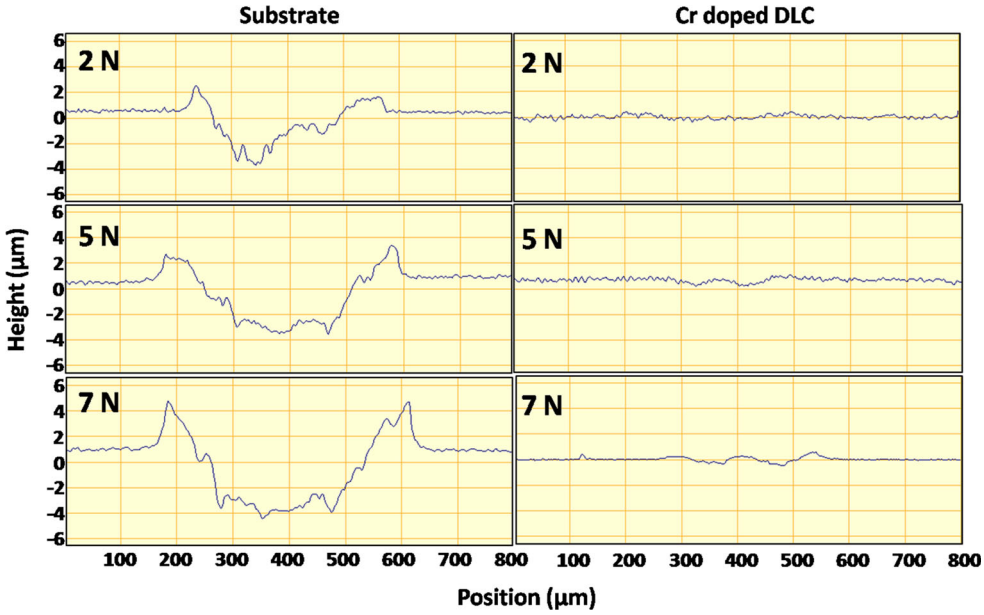

Fig. 12 2D profiles of wear tracks at 2, 5 and 7 N loads on substrate and 3.8% Cr-doped DLC-coated substrate

Table 5 Coefficient of friction (COF) and wear loss for substrate and 3.8% Cr-doped DLC samples

	Average coefficient of friction			Wear loss, mm^3		
Samples	**2 N**	**5 N**	**7 N**	**2 N**	**5 N**	**7 N**
Substrate	0.46	0.48	0.51	0.0100	0.0160	0.0220
3.8% Cr-DLC	0.15	0.15	0.16	0.00014	0.0008	0.0012

from abrasive wear with high COF and high wear loss on the substrate to a mild adhesive wear on the 3.8% Cr-doped DLC-coated substrate, particularly at low loads.

4. Conclusions

Cr-doped DLC coatings have been deposited on stainless steel and silicon substrates with different chromium concentrations. I_D/I_G ratio decreases with Cr doping up to 10.6%, and then it increases at 17.6% Cr, indicating that disorder gets enhanced in the DLC coating with very high Cr concentration. XPS studies demonstrate the presence of Cr carbide and Cr^{3+} species in the Cr-doped DLC coatings. At lower Cr contents Cr^{3+} dominates, whereas carbide species is more at higher Cr concentrations. However, carbide species are mainly present in the coatings after successive sputtering. DLC coating with Cr concentration of 3.8% shows good hardness, corrosion resistance and wear resistance properties. It shows hardness value of 22.6 GPa. Potentiodynamic polarization studies demonstrate that pure DLC and Cr-doped DLC coatings show better corrosion and passivation behavior compared to that of the substrate. Wear studies reveal a low friction coefficient of 0.15 and an order of magnitude lower wear rate of the Cr-doped DLC as compared to uncoated one.

Acknowledgments

The work was carried out under the CSIR network Project ESC-01-01. The authors would like to thank the Director, CSIR-National Aerospace Laboratories, Bengaluru, for his support and permission to publish the work. The authors would like to thank Mr. Siju John, Mr. N. T. Manikandanath and Mr. Muniprakash for FESEM, Raman spectroscopy and wear studies, respectively.

References

1. J. Fontaine, C. Donnet, and A. Erdemir, Fundamentals of the Tribology of DLC Coatings, *Tribology of Diamond-Like Carbon Films: Fundamentals and Applications*, C. Donnet and A. Erdemir, Ed., Springer, New York, 2008, p 139–154
2. J. Robertson, Diamond Like Amorphous Carbon, *Mater. Sci. Eng. R*, 2002, **37**, p 129–281
3. A. Erdemir, J. Vižintin, M. Kalin, K. Dohda, and S. Jahanmir, Ed., *Tribology of Mechanical Systems: A Guide to Present and Future Technologies*, ASME Press, New York, 2004, p 139
4. A. Grill, Diamond Like Carbon: State of The Art, *Diamond Relat. Mater.*, 1999, **8**, p 428–434
5. C. Donnet and A. Grill, Friction Control of Diamond Like Carbon Coatings, *Surf. Coat. Technol.*, 1997, **94**, p 456–462
6. S.C.H. Kwok, P.C.T. Ha, D.R. McKenzie, M.M.M. Bilek, and P.K. Chu, Biocompatibility of Calcium and Phosphorus Doped Diamond-Like Carbon Thin Films Synthesized by Plasma Immersion Ion Implantation and Deposition, *Diamond Relat. Mater.*, 2006, **15**, p 893–897
7. X.Z. Ding, B.K. Tay, S.P. Lau, P. Zhang, and X.T. Zeng, Structural and Mechanical Properties of Ti-Containing Diamond-Like Carbon Films Deposited by Filtered Cathodic Vacuum Arc, *Thin Solid Films*, 2002, **408**, p 183–187
8. K.I. Schiffmann, Phenomena in Microwear Experiments on Metal-Free and Metal-Containing Diamond-Like Carbon Coatings: Friction Wear Fatigue and Plastic Deformation, *Surf. Coat. Technol.*, 2004, **177**, p 453–458

9. K. Bewilogua, R. Wittorf, H. Thomsen, and M. Weber, DLC Based Coatings Prepared by Reactive DC Magnetron Sputtering, *Thin Solid Films*, 2004, **447**, p 142–147
10. G. Gassner, P.H. Mayrhofer, J. Patscheider, and C. Mitterer, Thermal Stability of Nanocomposite CrC/a-C: H Thin Films, *Thin Solid Films*, 2007, **515**, p 5411–5417
11. S. Zhang, X.L. Bui, J. Jiang, and X. Li, Microstructure and Tribological Properties of Magnetron Sputtered nc-TiC/aC Nanocomposite, *Surf. Coat. Technol.*, 2005, **198**, p 206–211
12. A.Y. Wang, K.R. Lee, J.P. Ahn, and J.H. Han, Structure and Mechanical Properties of W Incorporated Diamond-Like Carbon Films Prepared by a Hybrid Ion Beam Deposition Technique, *Carbon*, 2006, **44**, p 1826–1832
13. I. Gerhards, C. Ronning, U. Vetter, H. Hofsäss, H. Gibhardt, G. Eckold, Q. Li, S.T. Lee, Y.L. Huang, and M. Seibt, Ion Beam Synthesis of Amorphous Carbon Thin Films Containing Metallic Nanoclusters, *Surf. Coat. Technol.*, 2002, **158**, p 114–119
14. S. Dub, Y. Pauleau, and F. Thièry, Mechanical Properties of Nanostructured Copper-Hydrogenated Amorphous Carbon Composite Films Studied by Nanoindentation, *Surf. Coat. Technol.*, 2004, **180**, p 551–555
15. V. Singh, V. Palshin, R.C. Tittsworth, and E.I. Meletis, Structure of Composite Cr-Containing Diamond-Like Carbon Thin Films, *Carbon*, 2006, **44**, p 1280–1286
16. C. Strondl, N.M. Carvalho, J.T.H.M. De Hosson, and G.J. Van der Kolk, Investigation on the Formation of Tungsten Carbide in Tungsten-Containing Diamond Like Carbon Coatings, *Surf. Coat. Technol.*, 2003, **162**, p 288–293
17. B. Feng, D.M. Cao, W.J. Meng, J. Xu, R.C. Tittsworth, L.E. Rehn, P.M. Baldo, and G.L. Doll, Characterization of Microstructure and Mechanical Behavior of Sputter Deposited Ti-Containing Amorphous Carbon Coatings, *Surf. Coat. Technol.*, 2001, **148**, p 153–162
18. W. Dai, H. Zheng, G.S. Wu, and A.Y. Wang, Effect of Bias Voltage on Growth Property of Cr-DLC Film Prepared by Linear Ion Beam Deposition Technique, *Vacuum*, 2010, **85**, p 231–235
19. W. Dai, G. Wu, and A.Y. Wang, Preparation Characterization and Properties of Cr-Incorporated DLC Films on Magnesium Alloy, *Diamond Relat. Mater.*, 2010, **19**, p 1307–1315
20. W. Dai, G. Wu, and A. Wang, Structure and Elastic Recovery of Cr-C: H Films Deposited by a Reactive Magnetron Sputtering Technique, *Appl. Surf. Sci.*, 2010, **257**, p 244–248
21. W. Dai, P. Ke, and A. Wang, Microstructure and Property Evolution of Cr-DLC Films with Different Cr Content Deposited by a Hybrid Beam Technique, *Vacuum*, 2011, **85**, p 792–797
22. W. Dai and A. Wang, Synthesis, Characterization and Properties of the DLC Films with Low Cr Concentration Doping by a Hybrid Linear Ion Beam System, *Surf. Coat. Technol.*, 2011, **205**, p 2882–2886
23. M.C. Chiu, W.P. Hsieh, W.Y. Ho, D.Y. Wang, and S.F. Shieu, Thermal Stability of Cr-Doped Diamond-Like Carbon Films Synthesized by Cathodic Arc Evaporation, *Thin Solid Films*, 2004, **476**, p 258–263
24. Y. Xiang, W. Cheng-biao, L. Yang, Y. De-yang, and F. Zhi-qiang, Cr-Doped DLC Films in Three Mid-Frequency Dual-Magnetron Power Modes, *Surf. Coat. Technol.*, 2006, **200**, p 6765–6769
25. J. Sun, Z.Q. Fu, W. Zhang, C.B. Wang, W. Yue, S.S. Lin, and M.J. Dai, Friction and Wear of Cr-Doped DLC Films under Different Lubrication Conditions, *Vacuum*, 2013, **94**, p 1–5
26. J.A. Colón Santana, R. Skomski, V. Singh, V. Palshin, A. Petukhov, Ya.B. Losovyj, A. Sokolov, P.A. Dowben, and I. Ketsman, Magnetism of Cr-Doped Diamond-Like Carbon, *J. Appl. Phys.*, 2009, **105**, art. no. 07A930. doi:10.1063/1.3072828
27. D. Wang and Y.Y. Chang, Structural and Electrical Properties of Cr Doped a-C: H Films Synthesized by a Cathodic-Arc Activated Deposition Process, *Surf. Coat. Technol.*, 2006, **200**, p 3170–3174
28. F. Zhang, S. Krishnaswamy, D. Fei, D.A. Rebinsky, and B. Feng, Ultrasonic Characterization of Mechanical Properties of Cr and W-Doped Diamond-Like Carbon Hard Coatings, *Thin Solid Films*, 2006, **503**, p 250–258
29. X. Fan, E.C. Dickey, S.J. Pennycook, and M.K. Sunkara, Z-Contrast Imaging and Electron Energy-Loss Spectroscopy Analysis of Chromium-Doped Diamond-Like Carbon Films, *Appl. Phys. Lett.*, 1999, **75**, p 2740–2742
30. H. Renondeau, R.I. Taylor, G.C. Smith, and A.A. Torrance, Friction and Wear Performance of Diamond-Like Carbon and Cr-Doped Diamond-Like Carbon Coatings in Contact with Steel Surfaces, *J. Eng. Tribol.*, 2008, **222**, p 231–240
31. C.W. Zou, H.J. Wang, L. Feng, and S.W. Xue, Effects of Cr Concentrations on the Microstructure, Hardness, and Temperature-Dependent Tribological Properties of Cr-DLC Coatings, *Appl. Surf. Sci.*, 2013, **286**, p 137–141
32. Y. Zhuang, X. Jiang, A.V. Rogachev, D.G. Piliptsou, B. Ye, G. Liu, T. Zhou, and A.S. Rudenkov, Influences of Pulse Frequency on the Structure and Anti-corrosion Properties of the a-C: Cr Films, *Appl. Surf. Sci.*, 2015, **351**, p 1197–1203
33. S. Gayathri, N. Kumar, R. Krishnan, T.R. Ravindran, S. Dash, A.K. Tyagi, and M. Sridharan, Influence of Cr Content on the Microstructural and Tribological Properties of PLD Grown Nanocomposite DLC-Cr Thin Films, *Mater. Chem. Phys.*, 2015, **167**, p 194–200
34. M. Jelinek, T. Kocourek, J. Zemek, J. Mikšovský, Š. Kubinová, J. Remsa, J. Kopeček, and K. Jurek, Chromium-Doped DLC for Implants Prepared by Laser-magnetron Deposition, *Mater. Sci. Eng. C*, 2015, **46**, p 381–386
35. W. Yang, Y. Guo, D. Xu, J. Li, P. Wang, P. Ke, and A. Wang, Microstructure and Properties of (Cr:N)-DLC Films Deposited by a Hybrid Beam Technique, *Surf. Coat. Technol.*, 2015, **261**, p 398–403
36. C.-H. Liang, C.-F. Huang, and H.-Y. Tsai, The Influence of Substrate Bias Voltages on Structure, Mechanical Properties and Anti-corrosion Performance of Cr Doped Diamond-Like Carbon Films Deposited by Steered Cathodic Arc Evaporation, *Thin Solid Films*, 2015, **597**, p 88–96
37. Z. Wu, X. Tian, G. Gui, C. Gong, S. Yang, and P.K. Chu, Microstructure and Surface Properties of Chromium-Doped Diamond-Like Carbon Thin Films Fabricated by High Power Pulsed Magnetron Sputtering, *Appl. Surf. Sci.*, 2013, **276**, p 31–36
38. M. Stern and A.L. Geary, Electrochemical Polarization I. A Theoretical Analysis of the Shape of Polarization Curves, *J. Electrochem. Soc.*, 1957, **104**, p 56–63
39. Standard Test Method for Linearly Reciprocating Ball-on-Flat Sliding Wear, ASTM G133-02
40. P. Kumar, P.D. Babu, L. Mohan, C. Anandan, and V.K.W. Grips, Wear and Corrosion Behavior of Zr-Doped DLC on Ti-13Zr-13Nb Biomedical Alloy, *J. Mater. Eng. Perform.*, 2013, **22**, p 283–293
41. L. Mohan, P.D. Babu, P. Kumar, and C. Anandan, Influence of Zirconium Doping on the Growth of Apatite and Corrosion Behavior of DLC-Coated Titanium Alloy Ti-13Nb-13Zr, *Surf. Interface Anal.*, 2013, **45**, p 1785–1791
42. C. Anandan, L. Mohan, and P.D. Babu, Electrochemical Studies and Growth of Apatite on Molybdenum Doped DLC Coatings on Titanium Alloy B-21S, *Appl. Surf. Sci.*, 2014, **296**, p 86–94
43. F.C. Tai, S.C. Lee, J. Chen, C. Wei, and S.H. Chang, Multipeak Fitting Analysis of Raman Spectra on DLCH Film, *J. Raman Spectrosc.*, 2009, **40**, p 1055–1059
44. S. Gayathri, N. Kumar, R. Krishnan, T.R. Ravindran, S. Amirthapandian, S. Dash, A.K. Tyagi, and M. Sridharan, Influence of Transition Metal Doping on the Tribological Properties of Pulsed Laser Deposited DLC Films, *Ceram. Int.*, 2015, **41**, p 1797–1805
45. A.C. Ferrari and J. Robertson, Resonant Raman Spectroscopy of Disordered Amorphous and Diamond Like Carbon, *Phys. Rev. B*, 2001, **64**, art. no. 075414. doi:10.1103/PhysRevB.64.075414
46. G. Irmer and A. Dorner-Reisel, Micro-Raman Studies on DLC Coatings, *Adv. Eng. Mater.*, 2005, **7**, p 694–705
47. A.P. Piedade, J. Nunes, and M.T. Vieira, Thin Films with Chemically Graded Functionality Based on Fluorine Polymers and Stainless Steel, *Acta Biomater.*, 2008, **4**, p 1073–1080
48. K. Nygren, M. Samuelsson, A. Flink, H. Ljungcrantz, Å.K. Rudolphi, and U. Jansson, Growth and Characterization of Chromium Carbide Films Deposited by High Rate Reactive Magnetron Sputtering for Electrical Contact Applications, *Surf. Coat. Technol.*, 2014, **260**, p 326–334
49. S. Santra, P.K. Hota, R. Bhattarcharyya, P. Bera, P. Ghosh, and S.K. Mandal, Palladium Nanoparticles on Graphite Oxide: A Recyclable Catalyst for the Synthesis of Biaryl Cores, *ACS Catal.*, 2013, **3**, p 2776–2789
50. R. Younesi, P. Norby, and T. Vegge, A New Look at the Stability of Dimethyl Sulfoxide and Acetonitrile in Li-O_2 Batteries, *ECS Electrochem. Lett.*, 2014, **3**, p A15–A18
51. Z. Zhao, H. Zheng, Y. Wang, S. Mao, J. Niu, Y. Chen, and M. Shang, Synthesis of Chromium Carbide (Cr_3C_2) Nanopowders by the Carbonization of the Precursor, *J. Refract. Met. Hard Mater.*, 2011, **29**, p 614–617

52. J.F. Moulder, W.F. Stickle, P.E. Sobol, and K.D. Bomben, *Handbook of X-Ray Photoelectron Spectroscopy*, J. Chastain, Ed., Perkin-Elmer, Eden Prairie, 1992,
53. R. Teghil, A. Santagata, A. De Bonis, A. Galasso, and P. Villani, Chromium Carbide Thin Films Deposited by Ultra-Short Pulse Laser Deposition, *Appl. Surf. Sci.*, 2009, **255**, p 7729–7733
54. L. Ji, H. Li, F. Zhao, J. Chen, and H. Zhou, Microstructure and Mechanical Properties of Mo/DLC Nanocomposite Films, *Diamond Relat. Mater.*, 2008, **17**, p 1949–1954
55. R. Paul, A. Dey, A.K. Mukherjee, S.N. Sarangi, and A.K. Pal, Effect of Nanocrystalline Silver Impregnation on Mechanical Properties of Diamond-Like-Carbon Films by Nanoindentation, *Indian J. Pure Appl. Phys.*, 2012, **50**, p 252–259
56. W.H. Kao, Optimized aC Coatings by Doping with Zirconium for Tribological Properties and Machining Performance, *Diamond Relat. Mater.*, 2007, **16**, p 1896–1904
57. Y.F. Zheng, X.L. Liu, and H.F. Zhang, Properties of Zr-ZrC-ZrC/DLC Gradient Films on TiNi Alloy by The PIIID Technique Combined with PECVD, *Surf. Coat. Technol.*, 2008, **202**, p 3011–3016
58. J.C. Sánchez-López and A. Fernández, Doping and Alloying Effects on DLC Coatings, *Tribology of Diamond-Like Carbon Films: Fundamentals and Applications*, C. Donnet and A. Erdemir, Ed., Springer, New York, 2008, p 311–338
59. D. Caschera, F. Federici, S. Kaciulis, L. Pandolfi, A. Cusma, and G. Padeletti, Deposition of Ti-Containing Diamond-Like Carbon (DLC) Films by PECVD Technique, *Mater. Sci. Eng., C*, 2007, **27**, p 1328–1330